EUROPEAN ORGANIZATION FOR NUCLEAR RESEARCH (CERN)

CERN-EP-2022-031
2022/05/19

CMS-SUS-21-002

Search for electroweak production of charginos and neutralinos at $\sqrt{s} = 13\,\text{TeV}$ in final states containing hadronic decays of WW, WZ, or WH and missing transverse momentum

The CMS Collaboration

Abstract

This Letter presents a search for direct production of charginos and neutralinos via electroweak interactions. The results are based on data from proton-proton collisions at a center-of-mass energy of 13 TeV collected with the CMS detector at the LHC, corresponding to an integrated luminosity of $137\,\text{fb}^{-1}$. The search considers final states with large missing transverse momentum and pairs of hadronically decaying bosons WW, WZ, and WH, where H is the Higgs boson. These bosons are identified using novel algorithms. No significant excess of events is observed relative to the expectations from the standard model. Limits at the 95% confidence level are placed on the cross section for production of mass-degenerate wino-like supersymmetric particles $\widetilde{\chi}_1^{\pm}$ and $\widetilde{\chi}_2^0$, and mass-degenerate higgsino-like supersymmetric particles $\widetilde{\chi}_1^{\pm}$, $\widetilde{\chi}_2^0$, and $\widetilde{\chi}_3^0$. In the limit of a nearly-massless lightest supersymmetric particle $\widetilde{\chi}_1^0$, wino-like particles with masses up to 870 and 960 GeV are excluded in the cases of $\widetilde{\chi}_2^0 \to \text{Z}\widetilde{\chi}_1^0$ and $\widetilde{\chi}_2^0 \to \text{H}\widetilde{\chi}_1^0$, respectively, and higgsino-like particles are excluded between 300 and 650 GeV.

Submitted to Physics Letters B

1 Introduction

Supersymmetry (SUSY) [1–10] proposes to extend the standard model (SM) of particle physics by the addition of a new symmetry. This new symmetry requires that, for each boson (fermion) in the SM, there is also a fermionic (bosonic) superpartner, also called a "sparticle". SUSY can naturally predict cancellations of large radiative corrections to the Higgs boson (H) mass if some sparticles are not too heavy [11]. Recent work [12, 13] suggests that strongly interacting sparticles significantly heavier than current bounds [14–28] are consistent with a natural theory [11]. Contrastingly, charginos and neutralinos are still expected to be lighter than $\sim$1 TeV, with the lightest having a mass close to that of the Higgs boson. This suggests that the hunt for TeV-scale charginos and neutralinos is the next proving ground for natural SUSY.

In this Letter, we present a search for direct electroweak production of sparticles at the CERN LHC. The superpartners of the gauge bosons of the unbroken SU(2) and U(1) symmetries and the superpartners of the Higgs bosons (the winos, bino, and higgsinos, respectively) mix to form two chargino ($\widetilde{\chi}_i^{\pm}$ with $i = 1, 2$) and four neutralino ($\widetilde{\chi}_i^0$ with $i = 1, 2, 3, 4$) mass eigenstates, where i is in order of increasing mass. In the case where the mass mixing of the charginos and neutralinos is nearly diagonal, each of the mass eigenstates is identified as bino-, wino-, or higgsino-like, depending on the dominant contribution [10].

We search for direct production of wino-like charginos and neutralinos ($\widetilde{\chi}_1^{\pm}$ and $\widetilde{\chi}_2^0$) or higgsino-like charginos and neutralinos ($\widetilde{\chi}_1^{\pm}$, $\widetilde{\chi}_2^0$, and $\widetilde{\chi}_3^0$). We assume that the superpartners of the SM leptons are much heavier than the charginos and neutralinos. As such, decays of wino- or higgsino-like charginos and neutralinos proceed through W, Z, and Higgs bosons.

In this search, we assume that R-parity [29] is conserved and that the lightest neutralino is a bino-like $\widetilde{\chi}_1^0$ that is stable and will escape the detector unobserved. Such a $\widetilde{\chi}_1^0$ would be a viable candidate for weakly-interacting massive particle dark matter. We explore four signal regions, which target three prominent signatures when the scalar sparticles are very heavy: WW, WZ, or WH, together with a large transverse momentum imbalance.

At the LHC, several searches for direct chargino-neutralino and chargino-pair production in these channels have been performed by the ATLAS [30–38] and CMS [39–45] Collaborations. Most of these searches have been performed in events with at least one lepton. The present search is performed in fully hadronic final states, which feature larger branching fractions but larger backgrounds. Previous searches in fully hadronic final states have been performed for electroweak production of SUSY in the di-Higgs and other diboson channels by the ATLAS [37, 46] and CMS [47, 48] Collaborations. In this search we utilize machine learning algorithms to identify hadronically decaying high transverse momentum (p_T) W, Z, and Higgs bosons reconstructed as large-radius jets [49]. The search uses a sample of LHC proton-proton (pp) collisions at $\sqrt{s} = 13$ TeV collected by the CMS experiment between 2016 and 2018, corresponding to an integrated luminosity of 137 fb^{-1}. Tabulated results are provided in the HEPData record for this search [50].

2 Simulated event samples

Simulations of SM processes are used for optimizing selection criteria and computing several correction factors. These factors are used to predict the rates of SM backgrounds based on observations in various control regions. The production of $t\bar{t}$ + jets, W + jets, Z + jets, Drell–Yan, and quantum chromodynamics (QCD) multijet events is simulated at leading order (LO) using the MADGRAPH5_aMC@NLO (2.2.2 for 2016 and 2.4.2 for 2017–2018) generator [51]. The

$t\bar{t}$ + jets events are simulated with up to three additional partons at the matrix-element level, while the other samples are simulated with up to four additional partons at the matrix-element level. Single top quark events for all channels are modeled at next-to-leading order (NLO) in perturbative QCD. The MADGRAPH5_aMC@NLO generator is used for *s*-channel production of single top quark events, while POWHEG v1.0 (v2.0) [52–56] is used to simulate *t*-channel and associated tW production for 2016 (2017–2018). Additional small backgrounds, such as $t\bar{t}$ produced in association with one or more SM bosons, are similarly produced at NLO with either MADGRAPH5_aMC@NLO or POWHEG [57–59]. Events for 2016 (2017–2018) are generated using the NNPDF 3.0 (3.1) [60, 61] set of parton distribution functions. Parton showering and fragmentation are performed using the PYTHIA 8.2 [62] program with the underlying event models detailed in Refs. [63, 64]. The detector simulation is performed with GEANT4 [65]. The cross sections used to normalize most of the SM samples correspond to next-to-NLO precision in QCD.

Signal events are generated with the MADGRAPH5_aMC@NLO generator at LO precision in a similar manner to the SM backgrounds, with up to two additional partons at the matrix-element level. The detector simulation of signal samples is performed with the CMS fast simulation package [66, 67]. The signal samples are corrected for differences with respect to the GEANT4-based simulation. Both the SM background samples and the signal samples are generated with nominal distributions of additional pp interactions per bunch crossing, referred to as pileup, which are then rescaled to match the observed pileup distribution. The cross sections used for normalizing the signal yields are computed at NLO plus next-to-leading logarithmic precision [68, 69].

We interpret our results in terms of simplified models [70–74] with the assumption that a chargino pair $\widetilde{\chi}_1^{\pm}\widetilde{\chi}_1^{\mp}$ or a chargino-neutralino pair $\widetilde{\chi}_1^{\pm}\widetilde{\chi}_2^0$ is produced. In the simplified model scenarios, the chargino always decays to a W boson and the $\widetilde{\chi}_1^0$, while the neutralinos decay 100% of the time to either a Z or Higgs boson plus the $\widetilde{\chi}_1^0$, where the $\widetilde{\chi}_1^0$ is assumed to be the lightest supersymmetric particle (LSP), as depicted in Fig. 1. The simplified models are "TChiWW", $\widetilde{\chi}_1^{\pm}\widetilde{\chi}_1^{\mp}$ production with $\widetilde{\chi}_1^{\pm}$ decaying to a W boson and $\widetilde{\chi}_1^0$; "TChiWZ", $\widetilde{\chi}_1^{\pm}\widetilde{\chi}_2^0$ production with $\widetilde{\chi}_2^0$ decaying to a Z boson and $\widetilde{\chi}_1^0$; and "TChiWH", $\widetilde{\chi}_1^{\pm}\widetilde{\chi}_2^0$ production with $\widetilde{\chi}_2^0$ decaying to a Higgs boson and $\widetilde{\chi}_1^0$. In the TChiWZ and TChiWH scenarios, the $\widetilde{\chi}_1^{\pm}$ and $\widetilde{\chi}_2^0$ are the mass-degenerate next-to-lightest supersymmetric particles (NLSPs), while in the TChiWW scenario, the $\widetilde{\chi}_1^{\pm}$ is the NLSP. For these scenarios, we assume the $\widetilde{\chi}_1^{\pm}$ and $\widetilde{\chi}_2^0$ to be purely wino-like.

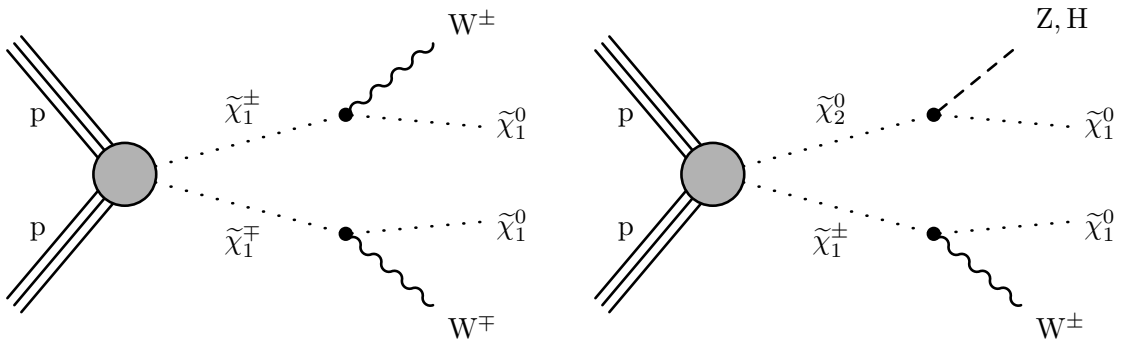

Figure 1: Diagrams for the production of $\widetilde{\chi}_1^{\pm}\widetilde{\chi}_1^{\mp}$ and $\widetilde{\chi}_1^{\pm}\widetilde{\chi}_2^0$ with the $\widetilde{\chi}_1^{\pm}$ decaying to a W boson and $\widetilde{\chi}_1^0$ and the $\widetilde{\chi}_2^0$ decaying to either a Z boson or a Higgs boson and $\widetilde{\chi}_1^0$.

In addition to these simplified models, we also consider two more specific scenarios in which

all of the winos or all of the higgsinos are mass degenerate, which we refer to as the wino- and higgsino-like NLSP scenarios. For the wino-like NLSP scenario, we assume a mass-degenerate $\widetilde{\chi}_1^{\pm}\widetilde{\chi}_2^0$ pair with a lighter bino-like $\widetilde{\chi}_1^0$ as the LSP. In this scenario, both $\widetilde{\chi}_1^{\pm}\widetilde{\chi}_1^{\mp}$ and $\widetilde{\chi}_1^{\pm}\widetilde{\chi}_2^0$ production are expected and would contribute to the targeted signatures, so these two production processes are combined and searched for simultaneously. We consider two options for the decay of the $\widetilde{\chi}_2^0$: either $\widetilde{\chi}_2^0 \to \mathrm{Z}\widetilde{\chi}_1^0$ or $\widetilde{\chi}_2^0 \to \mathrm{H}\widetilde{\chi}_1^0$, with 100% branching fraction in each case. For the higgsino-like NLSP scenario, we assume mass-degenerate $\widetilde{\chi}_1^{\pm}$, $\widetilde{\chi}_2^0$, and $\widetilde{\chi}_3^0$ with a lighter bino-like $\widetilde{\chi}_1^0$. In this scenario, the production of $\widetilde{\chi}_1^{\pm}\widetilde{\chi}_1^{\mp}$, $\widetilde{\chi}_1^{\pm}\widetilde{\chi}_2^0$, $\widetilde{\chi}_1^{\pm}\widetilde{\chi}_3^0$, and $\widetilde{\chi}_2^0\widetilde{\chi}_3^0$ are combined and searched for simultaneously. We assume 100% branching fractions of $\widetilde{\chi}_2^0 \to \mathrm{Z}\widetilde{\chi}_1^0$ and $\widetilde{\chi}_3^0 \to \mathrm{H}\widetilde{\chi}_1^0$ as expected for scenarios with $\tan\beta \sim 1$ [75, 76]. We consider signal events with WW, WZ, WH, or ZH and large $p_{\mathrm{T}}^{\mathrm{miss}}$. The WW, WZ, and WH events arise from $\widetilde{\chi}_1^{\pm}\widetilde{\chi}_1^{\mp}$, $\widetilde{\chi}_1^{\pm}\widetilde{\chi}_2^0$, or $\widetilde{\chi}_1^{\pm}\widetilde{\chi}_3^0$ production. The ZH events arise from $\widetilde{\chi}_2^0\widetilde{\chi}_3^0$ production. All the other sparticles are assumed to be too heavy to affect the production of charginos and neutralinos [68, 69].

3 The CMS detector and event reconstruction

A detailed description of the CMS detector, together with a definition of the coordinate system used and the relevant kinematic variables, can be found in Ref. [77]. Briefly, a superconducting solenoid of 6 m internal diameter provides a magnetic field of 3.8 T. Within the solenoid volume are a silicon pixel and strip tracker covering pseudorapidity $|\eta| < 2.5$, a lead tungstate crystal electromagnetic calorimeter, and a brass and scintillator hadron calorimeter, each composed of a barrel and two endcap sections and covering $|\eta| < 3$. Forward calorimeters extend the pseudorapidity coverage to include $3 < |\eta| < 5.2$. Muons are detected in gas-ionization chambers embedded in the steel flux-return yoke outside the solenoid.

The particle-flow (PF) algorithm [78] combines all detector subsystems to identify and reconstruct charged and neutral hadrons, photons, electrons, and muons. This analysis utilizes PF jets, which are produced by clustering PF candidates into anti-k_{T} [79, 80] jets. We utilize two jet collections in which the clustering size is either 0.4 (AK4 jets) or 0.8 (AK8 jets). The latter is well-suited for reconstructing hadronic decays of W, Z, and Higgs bosons with $p_{\mathrm{T}} > 200\,\mathrm{GeV}$. We correct the jets for pileup effects [81, 82] and the jet energy scale [83]. The AK8 jet mass m_{J} is calculated using the soft-drop algorithm [84]. We consider only AK4 jets with $p_{\mathrm{T}} > 30\,\mathrm{GeV}$ and $|\eta| < 2.4$ and AK8 jets with $p_{\mathrm{T}} > 200\,\mathrm{GeV}$ and $|\eta| < 2$ that satisfy a set of quality criteria to eliminate jets from spurious sources, such as electronics noise [81].

The variable $\vec{p}_{\mathrm{T}}^{\,\mathrm{miss}}$ is defined as the negative vector sum of $\vec{p}_{\mathrm{T}}$ for all PF candidates, and its magnitude is denoted by $p_{\mathrm{T}}^{\mathrm{miss}}$. Known detector effects are accounted for by adjusting $p_{\mathrm{T}}^{\mathrm{miss}}$ for jet energy corrections [85]. A set of quality criteria is used to identify and eliminate events in which detector noise, inoperable calorimeter cells, beam halo, and other effects mimic $p_{\mathrm{T}}^{\mathrm{miss}}$ [85].

The identification of jets originating from a bottom quark (b tagging) is performed by applying a version of the combined secondary vertex algorithm that utilizes deep-learning techniques [86]. For the medium working point utilized in this search, the efficiency of tagging b jets with $p_{\mathrm{T}} > 30\,\mathrm{GeV}$, as measured in $\mathrm{t\bar{t}}$ events, is about 68%; the probability of misidentifying jets arising from the hadronization of a charm quark is roughly 12% and for jets from a light-flavor quark or a gluon it is roughly 1%.

The lepton content of events is used to separate the fully hadronic signal samples from the single-lepton control samples, as described in Sections 4 and 5. We require electron and muon candidates [87, 88] to have $p_{\mathrm{T}} > 10\,\mathrm{GeV}$ and to lie within $|\eta| < 2.5$ for electrons and $|\eta| < 2.4$ for muons. Electron candidates are required to satisfy the "veto" requirements described in

Ref. [87], and muon candidates are required to satisfy the "medium" requirements described in Ref. [88]. We also impose isolation requirements on electron and muon candidates to suppress those arising from jets erroneously identified as leptons, as well as genuine leptons from hadron decays, using the same criteria as in Refs. [22, 89]. To recover electrons or muons that fail the identification requirements, as well as τ leptons via their one-prong hadronic decays, we make use of isolated tracks. Isolated tracks are required to satisfy $|\eta| < 2.4$ and $p_T > 5\,\text{GeV}$ for PF electrons and muons, and $p_T > 10\,\text{GeV}$ for PF hadrons [22].

Photon candidates, which are only used to remove events from the data set as described in Section 4, are required to have $p_T > 100\,\text{GeV}$ and $|\eta| < 2.4$ and to be isolated from charged hadrons, neutral hadrons, and electromagnetic particles [90].

Candidate AK8 jets consistent with the decay and subsequent fragmentation and hadronization of heavy SM bosons are identified using a deep neural network (DNN). The DNN is designed to classify AK8 jets arising from hadronically decaying particles of five main categories: W, Z, H, t, and "other". Jets are further classified into subcategories according to their likelihood of originating from specific decays of these unstable particles, e.g., $Z(b\bar{b})$, $Z(c\bar{c})$, etc. The architecture of the DNN and details of its training can be found in Ref. [49]. Each classification has a corresponding score that is used to develop jet taggers.

In this analysis, three jet taggers, which were developed from these classifiers, are used to categorize AK8 jets: the W tagger, the V tagger, and the $b\bar{b}$ tagger. These taggers are non-exclusive, i.e., a single AK8 jet may be tagged by any, all, or none of the three taggers. Each tagger involves the DNN and the jet mass. The W tagger identifies jets consistent with a $W(q\bar{q}')$ decay by their mass ($65 < m_J < 105\,\text{GeV}$) and a DNN score optimized for distinguishing between hadronic W boson decays and QCD jets. The V tagger identifies jets consistent with a $W(q\bar{q}')$ or $Z(q\bar{q})$ decay by their mass ($65 < m_J < 105\,\text{GeV}$) and a DNN score optimized in a similar manner to the W tagger, but utilizing adversarial training [91] to decorrelate the DNN score and the jet mass, which allows the V tagger to be sensitive to the hadronic decays of both the W and Z bosons. The $b\bar{b}$ tagger identifies AK8 jets consistent with a $Z(b\bar{b})$ or $H(b\bar{b})$ decay by their mass ($75 < m_J < 140\,\text{GeV}$) and a DNN score optimized for identifying Lorentz-boosted $b\bar{b}$ topologies. The $b\bar{b}$ tagger also utilizes adversarial training to decorrelate the DNN score and the jet mass. The $b\bar{b}$ tagger has an efficiency of about 54% for jets with $p_T > 300\,\text{GeV}$ originating from Higgs or Z bosons decaying into $b\bar{b}$, and a misidentification rate of roughly 2.5% for QCD jets. Similarly, the W tagger has an efficiency of about 41% for jets arising from hadronic W boson decays and a misidentification rate of roughly 1%, and the V tagger has an efficiency of about 45% for tagging hadronic W and Z boson decays and a misidentification rate of roughly 2.5%.

4 Triggers and event selection

Candidate events are recorded based on a trigger [92] that requires p_T^{miss} to be larger than a time-dependent threshold that varies between 90 and 140 GeV. The efficiency of these triggers is measured using a separate data set in which events are recorded based on the requirement that a single electron or single muon is reconstructed. For p_T^{miss} of about 200 GeV, which is the minimum p_T^{miss} used in this search, the trigger efficiency is found to be 95, 78, and 74% for the 2016, 2017, and 2018 data-taking periods, respectively. This variation in the trigger efficiency is caused by the changes in the trigger threshold over time, but the efficiency rises above 98% for $p_T^{\text{miss}} > 270\,\text{GeV}$ for all years. When computing event yields, parameterizations of these efficiencies are used to correct simulations. For ancillary measurements of jet tagging rates in

the data, a combination of single-lepton and dilepton triggers is used.

All events in our signal regions (SRs) are required to satisfy a common set of baseline selection criteria. Each event is required to have a primary vertex [93] and no isolated leptons, isolated photons, or isolated tracks. Leptons, in particular, typically arise from a W boson decay, which constitutes a major background. The requirement of no leptons in our SRs makes this analysis orthogonal to other searches targeting common signals in final states that include leptons [39–43]. Events containing isolated tracks are only removed from the data set if the transverse mass based on the track satisfies $m_{\mathrm{T}} = \sqrt{2 p_{\mathrm{T}} p_{\mathrm{T}}^{\mathrm{miss}} (1 - \cos\Delta\phi)} < 100\,\mathrm{GeV}$, where $\Delta\phi$ refers to the azimuthal separation between the track and $\vec{p}_{\mathrm{T}}^{\,\mathrm{miss}}$ directions. Low m_{T} is typical of tracks from $\mathrm{W} \to \ell\nu$ decays but less common in signal events with isolated tracks. Events are required to have $p_{\mathrm{T}}^{\mathrm{miss}} > 200\,\mathrm{GeV}$ and $H_{\mathrm{T}} > 300\,\mathrm{GeV}$, where H_{T} is defined as the scalar sum of p_{T} for all AK4 jets which satisfy the kinematic and quality criteria mentioned in Section 3. Large $p_{\mathrm{T}}^{\mathrm{miss}}$ and H_{T} values are typical of chargino and neutralino production when a high-momentum boson is present. Signal events typically have two AK8 jets and four AK4 jets (note that AK4 jets may overlap AK8 jets); accordingly we require at least two AK8 jets and 2–6 (inclusive) AK4 jets. We also impose requirements on the azimuthal angle $\Delta\phi_{\mathrm{i}}$ between $\vec{p}_{\mathrm{T}}^{\,\mathrm{miss}}$ and each of the four highest p_{T} AK4 jets, where the subscript i refers to the p_{T} ordering of the jets. Each event must satisfy $\Delta\phi_{1,2,3,4} > 1.5, 0.5, 0.3$, and 0.3. Events must satisfy $\Delta\Phi_{1,2} > 1.5$ and 0.5, where $\Delta\Phi_{\mathrm{i}}$ is defined analogously to $\Delta\phi_{\mathrm{i}}$ using the two highest p_{T} AK8 jets. These requirements on azimuthal angles suppress the background from QCD multijet events, for which $\vec{p}_{\mathrm{T}}^{\,\mathrm{miss}}$ is usually aligned along a jet direction. Within this baseline phase space, four SRs are defined. One SR requires zero b-tagged AK4 jets ($n_{\mathrm{b}} = 0$), which we refer to as the b-veto region. The remaining three SRs require at least one b-tagged AK4 jet ($n_{\mathrm{b}} \geq 1$), which we refer to as the b-tag regions. In addition to these SRs, we also define several control regions (CRs), which are used to help constrain the background estimates, as described in Section 5.

4.1 The b-veto search region

The b-veto SR seeks to isolate events that are consistent with the production of WW or WZ pairs of bosons, along with a large $p_{\mathrm{T}}^{\mathrm{miss}}$. In addition to the baseline event selection described above, the b-veto SR requires that at least two AK8 jets satisfy $65 < m_{\mathrm{J}} < 105\,\mathrm{GeV}$. At least one AK8 jet must be W tagged, and at least one other AK8 jet must be V tagged, as described in Section 3. A summary of the b-veto SR requirements is shown in Table 1. The b-veto SR is further subdivided into nine bins of $p_{\mathrm{T}}^{\mathrm{miss}}$. The lower $p_{\mathrm{T}}^{\mathrm{miss}}$ bin boundaries are 200, 250, 300, 350, 400, 450, 500, 600, and 800 GeV.

Table 1: Summary of tagging requirements for the b-veto SR and CRs. Each of these regions includes the baseline selection described in Section 4 and requires zero b-tagged AK4 jets and at least two AK8 jets satisfying $65 < m_{\mathrm{J}} < 105\,\mathrm{GeV}$. The SR and CRs are described in detail in Sections 4.1 and 5.1, respectively. The W and V taggers are described in Section 3.

Region	Requirements
b-veto SR	$\geq$1 V-tagged jet $\geq$1 W-tagged jet $\geq$2 V- or W-tagged jets
b-veto 0-tag CR	0 V-tagged jets 0 W-tagged jets
b-veto 1-tag CR	1 V-tagged jet 0 other W-tagged jets

The main background in the b-veto SR arises from $W/Z+$jets production with $W \to \ell\nu$ or $Z \to \nu\bar{\nu}$. The $W \to \ell\nu$ background is substantially reduced by requiring the number of reconstructed charged leptons and isolated tracks to be zero. These events still satisfy the event selection criteria when the charged lepton lies outside the lepton acceptance, is not reconstructed, or is not isolated. In $W/Z+$jets background events, both W- and V-tagged AK8 jets arise from misidentification of jets not originating from hadronic W or Z boson decays. These events together with background events arising from QCD multijet production do not contain any resonance reconstructed as a single AK8 jet, and are referred to as the "0-res" background.

The next largest background contributions come from $t\bar{t}$, single top quark, and diboson production. These events typically have one leptonically decaying vector boson and one hadronically decaying vector boson. Therefore, one W- or V-tagged AK8 jet arises from a hadronic W or Z boson decay, and the other tag arises from misidentification. We refer to these backgrounds, which contain only one resonance reconstructed as a single AK8 jet, as the "1-res" backgrounds. The remaining minor background contributions, which constitute less than 10% of the expected event yield in any p_T^{miss} bin of the SR, are expected from rare processes such as triboson production and $t\bar{t}$ pairs produced in association with a W, Z, or Higgs boson.

The m_J distribution of V-tagged jets for signal, expected SM backgrounds, and observed event yields in the b-veto SR is shown in Fig. 2 (left), in which the mass requirement of the V tagger has been loosened to show the behavior of the signal and backgrounds in both the tagged regions and the sidebands. In some events, there are multiple V-tagged jets, some of which could also be W tagged. In such events, the jet that is both W and V tagged and has the highest W tagger DNN score is ignored, and the V-tagged jet with the highest V tagger DNN score among the remaining jets is plotted. The simulated event yields are scaled such that the yield within the SR matches our total SM background predictions, which will be described in Section 5. The distributions for the TChiWZ and TChiWW signals show peaks in the region of 65–105 GeV, corresponding to the mass requirement of the V tagger.

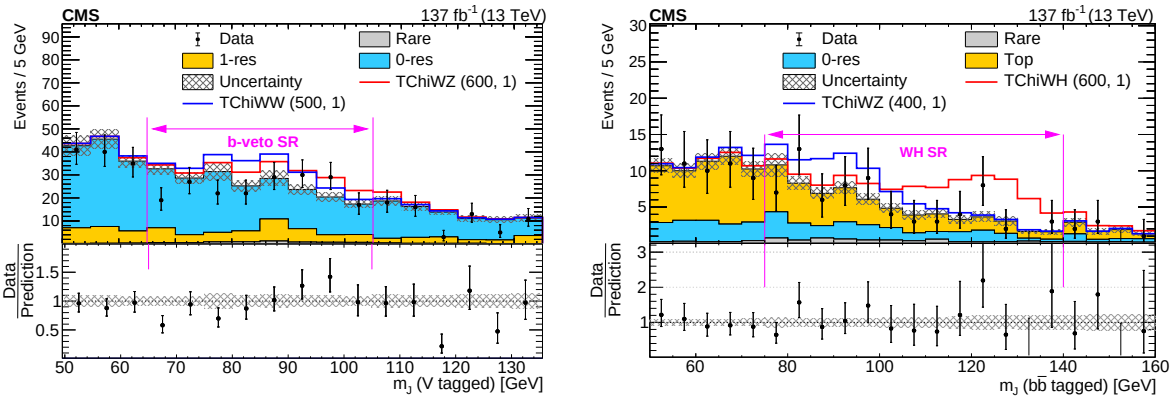

Figure 2: Distributions of the jet mass for V-tagged AK8 jets in the b-veto SR (left) and $b\bar{b}$-tagged AK8 jets in the WH SR (right). The jet mass requirements for the V and $b\bar{b}$ taggers have been loosened in these figures. The filled histograms show the SM background simulation, scaled such that the yield within the SR matches the total SM background predictions. The open histograms show the sum of the scaled SM background simulations and of the expectations for selected signal models, which are denoted in the legend by the name of the model followed by the assumed masses of the NLSP and LSP in GeV. The observed event yields are indicated by black markers. The hatched gray bands correspond to the statistical uncertainties in the SM predictions, but no systematic uncertainties are included.

Table 2: Summary of tagging requirements for the b-tag SRs and CRs. Each of these regions includes the baseline requirements described in Section 4 and requires at least one b-tagged AK4 jet and at least two AK8 jets. The SRs and CRs are described in detail in Sections 4.2 and 5.2, respectively. The $\mathrm{b\bar{b}}$ and W taggers are described in Section 3, and the definitions of W and Higgs boson candidates are given in Section 4.2. In addition to the six regions described in this table, the b-tag predictions also use six single-lepton CRs that are identical except that exactly one charged lepton is required. A dash (—) indicates that no requirement is imposed.

	W boson candidate		Higgs boson candidate	
	W tagged	not W tagged	$\mathrm{b\bar{b}}$ tagged	not $\mathrm{b\bar{b}}$ tagged
WH SR	$\geq$1	—	$\geq$1	—
W SR	$\geq$1	—	0	—
H SR	0	—	$\geq$1	—
WH antitag CR	0	$\geq$1	0	$\geq$1
W antitag CR	0	$\geq$1	0	0
H antitag CR	0	0	0	$\geq$1

4.2 The b-tag search regions

To maximize our acceptance of signal events, we define three SRs for events containing at least one b-tagged AK4 jet. These SRs are defined in terms of the numbers of "W boson candidates" and "Higgs boson candidates", which are AK8 jets selected according to m_{J} and according to their proximity to a b-tagged AK4 jet. An AK8 jet is said to contain a b-tagged AK4 jet if the event includes at least one b-tagged AK4 jet that satisfies $\Delta R(\text{b jet, AK8 jet}) < 0.8$, where $\Delta R = \sqrt{(\Delta\eta)^2 + (\Delta\phi)^2}$ is the distance in the pseudorapidity-azimuth plane. A W boson candidate is any AK8 jet that lies in the W/Z mass window $65 < m_{\mathrm{J}} < 105\,\mathrm{GeV}$ and does not contain a b-tagged jet. Similarly, a Higgs boson candidate is any AK8 jet that lies in the Z/H mass window $75 < m_{\mathrm{J}} < 140\,\mathrm{GeV}$ and contains at least one b-tagged jet. These two classes of AK8 jets do not overlap, but not every AK8 jet falls into either class. We further subdivide these classes based on jet tagging. The W tagger is used to divide W boson candidates into tagged and untagged subcategories, and the $\mathrm{b\bar{b}}$ tagger is similarly used to divide Higgs boson candidates into tagged and untagged subcategories.

The three SRs with b-tagged jets are referred to as the WH, W, and H SRs. These SRs isolate events in which a WH, WZ, or ZH pair of bosons is produced with large $p_{\mathrm{T}}^{\mathrm{miss}}$. The WH SR requires at least one tagged W boson candidate and at least one tagged Higgs boson candidate. The W SR requires at least one tagged W boson candidate and exactly zero tagged Higgs boson candidates, although untagged Higgs boson candidates are permitted. The H SR requires at least one tagged Higgs boson candidate and exactly zero tagged W boson candidates, but similarly imposes no requirement on untagged W boson candidates. These requirements are summarized in Table 2.

The SM backgrounds that contribute to the three b-tag SRs are top quark pair production, especially at low $p_{\mathrm{T}}^{\mathrm{miss}}$, and W/Z + jets events, especially at high $p_{\mathrm{T}}^{\mathrm{miss}}$. In all three b-tag SRs, there are small contributions from diboson and triboson production, as well as $\mathrm{t\bar{t}}$ production in association with a W, Z, or Higgs boson. The backgrounds containing top quarks include a mixture of events with one and two resonances each reconstructed as a single AK8 jet, and so we refer to these backgrounds in the b-tag region as "top" rather than as "1-res".

The b-tag SRs are also subdivided into bins of $p_{\mathrm{T}}^{\mathrm{miss}}$. The W and H SRs use the same $p_{\mathrm{T}}^{\mathrm{miss}}$ binning as the b-veto SR. For the WH SR, the last two $p_{\mathrm{T}}^{\mathrm{miss}}$ bins are merged because of the small expected number of events in the corresponding CRs.

The distribution of the Higgs boson candidate m_J for events in the WH SR for signal, expected SM backgrounds, and observed event yields is shown in Fig. 2 (right), in which the Higgs boson candidate mass requirement has been loosened by $\sim$20 GeV on either side to show the distribution both in and near the SR. The predicted yields from simulation are scaled such that the total SM background yields in the SR match the total prediction using the procedure described in Section 5. Distributions for the TChiWZ and TChiWH signals show peaks in the region of 75–140 GeV, corresponding to the Z and Higgs boson masses.

5 Background estimation

To constrain the contribution from the dominant SM processes in each of our SRs, several CRs are defined. Each CR has reduced contributions from signal processes and enhanced contributions from SM background processes. Most of our CRs isolate different background components by inverting various tagging requirements to select events with a misidentified boson. For the b-tag SRs, where backgrounds involving top quarks are more prominent, a combination of CRs with inverted tagging requirements and with one charged lepton is used.

5.1 Background estimation for the b-veto search region

The sum of 0- and 1-res background events in the b-veto SR is estimated simultaneously from two mutually-exclusive CRs. Both CRs require at least two AK8 jets that satisfy the WZ mass requirements. The 0-tag CR is defined by requiring that all AK8 jets satisfying the WZ mass requirements are neither W tagged nor V tagged. This CR is dominated by the 0-res background. The 1-tag CR requires exactly one V-tagged jet, and requires that all other AK8 jets that satisfy the WZ mass requirements are neither W tagged nor V tagged. The main contribution to the 1-tag CR also comes from the 0-res background, but this CR has increased contributions from the 1-res background compared to the 0-tag CR. The requirements for both b-veto CRs are summarized in Table 1.

The background yields in the b-veto SR are estimated using two sets of transfer factors derived from simulation, $\mathcal{R}_i$, defined as the ratio of the summed 0- and 1-res event yields in the SR divided by those in either the 0-tag ($\mathcal{R}_0$) or 1-tag CR ($\mathcal{R}_1$). The values of $\mathcal{R}_i$ are computed separately for each p_T^{miss} bin and typically range between 0.2 and 0.3. The contributions of rare processes to the SR and CRs are taken from simulation with appropriate data-to-simulation corrections applied [49, 83, 86]. The total background prediction is given by

$$N_{SR}^{pred} = \mathcal{R}_i(N_{CR_i}^{data} - N_{CR_i,rare}^{MC}) + N_{SR,rare}^{MC},$$

where N denotes the number of events expected (or observed in data) in regions and from processes indicated by the superscripts and subscripts, $\mathcal{R}_i = N_{SR,0\&1\text{-res}}^{MC}/N_{CR_i,0\&1\text{-res}}^{MC}$, and CR_i is either the 0- or 1-tag CR. The final background predictions for the SR are determined by a simultaneous fit of the two CRs. The background composition of the 1-tag CR is very similar to the b-veto SR, while the signal contamination is smaller in the 0-tag CR. Using both CRs allows us to benefit from these advantages.

The W and V tagging rates in simulation are corrected to match those measured in data. The corrections for jets matched to generator-level W bosons are obtained from a $t\bar{t}$-enriched sample in which one of the W bosons from the top quark decays leptonically and the other decays hadronically [49]. The same corrections are also applied to jets matched to generator-level Z bosons. The corrections for misidentified jets are obtained from a sample of events with an

$\ell^+\ell^-$ ($\ell = \mathrm{e}, \mu$) pair and at least one AK8 jet. The W- or V-tagged jets in these events are dominated by misidentification. Uncertainties associated with the determination of these corrections are propagated to the final predictions.

Our b-veto background prediction method relies on the modeling of the AK8 jet W- and V-tagging efficiencies in simulation after the corrections described above are applied. Several validation regions (VRs) are defined to check how well the simulation models the tagging efficiencies in the phase space close to our SR and CRs. For one set of VRs, events are required to satisfy the baseline event selection criteria except for the second AK8 jet requirement, and to have only one AK8 jet, which is W or V tagged. These VRs are referred to as the 1-jet W- and V-tag VRs, respectively. The predicted SM backgrounds, with the exception of the rare backgrounds, in each VR are based on an extrapolation from CRs defined by the inversion of the DNN requirement for the W or V tag compared to the corresponding VR. The predicted yields of the rare backgrounds are obtained directly from simulation, not via extrapolation from CRs. The predictions in these 1-jet VRs are found to be compatible with our observations.

Similar tests are also performed using events that satisfy the baseline event selection criteria including the requirement of having at least two AK8 jets but only one of them satisfying $65 < m_{\mathrm{J}} < 105\,\mathrm{GeV}$. These events are orthogonal to events in any of b-veto SR and CRs, as the b-veto SR and CRs require at least two jets to satisfy $65 < m_{\mathrm{J}} < 105\,\mathrm{GeV}$. We then require that only one AK8 jet is W or V tagged. These b-veto VRs are referred to as the 2-jet W- and V-tag VRs, respectively. Predictions of the background yields, with the exception of the rare backgrounds, are made by extrapolating from CRs defined by inversion of the tagging DNN requirement. As before the rare backgrounds yields are taken directly from simulation.

In the 2-jet W- and V-tag VRs, the observed event yields are higher than the SM background predictions, primarily in the intermediate- to high-$p_{\mathrm{T}}^{\mathrm{miss}}$ region, which may be attributed to a dependence of the misidentification rate corrections on event topology or on AK8 jet multiplicity in this phase space. We correct the background predictions in the b-veto SR to account for these discrepancies. The correction from the W-tag VR is applied to the extrapolation from the 1-tag CR to the SR, and the corrections from the W- and V-tag CRs are both applied to the extrapolation from the 0-tag CR to the SR. The corrections obtained from the 2-jet W- and V-tag VRs range from 1.03 and 1.01 at low $p_{\mathrm{T}}^{\mathrm{miss}}$ to 1.48 and 1.27 in the highest $p_{\mathrm{T}}^{\mathrm{miss}}$ bin, respectively. The full size of these corrections is considered as a systematic uncertainty.

5.2 Background estimation for the b-tag search regions

For each of the three b-tag SRs, we define three sets of CRs, for a total of nine CRs. The first set, the antitag CRs, inverts the boson tagging requirements of the corresponding SRs. In the antitag CRs, every Higgs boson candidate must not be $\mathrm{b\bar{b}}$ tagged, and every W boson candidate must not be W tagged. Otherwise, the definitions of the WH, W, and H antitag CRs, which are summarized in Table 2, are identical to the corresponding SRs. The antitag CRs are enhanced in $\mathrm{W/Z}+\mathrm{jets}$ but still have contributions from events containing top quarks.

The two remaining sets of CRs are defined identically to the SRs and antitag CRs but require exactly one lepton, i.e., there is a set of three single-lepton (1ℓ) tagged CRs and a set of three 1ℓ antitag CRs. The 1ℓ CRs feature enhanced rates of top quark pair production. A summary of the selection for each SR and corresponding CR is given in Table 2. All of the SRs and CRs are mutually non-overlapping.

The 1ℓ CRs are used to constrain the estimates of top quark backgrounds in the SRs and zero-lepton antitag CRs, while the antitag CRs are used to constrain the estimates of the 0-res back-

grounds in the SRs and tagged CRs.

The 1ℓ CRs are dominated by top quark pair production, with small contributions from W + jets and even smaller contributions from single top quark production and $\mathrm{t\bar{t}H}$. A transfer factor, $\mathcal{R}_{0\ell/1\ell}$, is used to provide an estimate of the number of top quark background events in either the SR or the 0ℓ antitag CR, where 0ℓ refers to the SRs and the antitag CRs with zero leptons. The values of $\mathcal{R}_{0\ell/1\ell}$ are computed from simulation, including all corrections to the lepton reconstruction efficiencies, b tagging efficiencies, and AK8 jet tagging efficiencies.

The predicted number of top quark background events in either the SR or the 0ℓ antitag CR is given by

$$N_{\mathrm{i,top}}^{\mathrm{pred},0\ell} = \frac{N_{\mathrm{i,top}}^{\mathrm{MC},0\ell}}{N_{\mathrm{i,all}}^{\mathrm{MC},1\ell}} N_{\mathrm{i}}^{\mathrm{data},1\ell} = \mathcal{R}_{0\ell/1\ell} N_{\mathrm{i}}^{\mathrm{data},1\ell}, \tag{1}$$

where N^{MC} denotes the number of events expected from simulation, N^{data} denotes the number of observed events, and N^{pred} denotes the number of events predicted via this method. Additionally, the subscript i denotes the tagging region, tag or antitag. The subscript "all" refers to all of the SM backgrounds, while "top" refers to only the top quark backgrounds.

A transfer factor $\mathcal{R}_{\mathrm{tag}}$ is used to constrain the 0-res event yields in the SR based on observations in the 0ℓ antitag CR. The value of $\mathcal{R}_{\mathrm{tag}}$ is computed using simulation and is the ratio of the number of 0-res events in the SR to the number of 0-res events in the 0ℓ antitag CR. This transfer factor does not include the top quark backgrounds, which are constrained separately via the 1ℓ CRs. The transfer factor is corrected for differences in tagging rates between simulation and data. Corrections are derived separately for W- and $\mathrm{b\bar{b}}$-tagged jets, and separately for misidentified and correctly tagged jets [49]. Corrections for misidentified jets are derived in a similar manner to the corrections used for the b-veto regions, using samples of Drell–Yan events and requiring $n_{\mathrm{b}} = 1$. All uncertainties in these corrections are propagated to the final predictions.

Using $\mathcal{R}_{\mathrm{tag}}$ and the prediction of the top quark backgrounds described above, the predicted 0-res background contribution to the SR is given by

$$N_{\text{0-res}}^{\mathrm{pred},0\ell} = \mathcal{R}_{\mathrm{tag}} \left(N_{\mathrm{antitag}}^{\mathrm{data},0\ell} - N_{\mathrm{antitag,top}}^{\mathrm{pred},0\ell} - N_{\mathrm{antitag,rare}}^{\mathrm{MC},0\ell} \right), \tag{2}$$

where $N_{\mathrm{antitag}}^{\mathrm{data},0\ell}$ denotes the number of observed events in the 0ℓ antitag CR, $N_{\mathrm{antitag,top}}^{\mathrm{pred},0\ell}$ denotes the predicted number of top quark background events from Eq. (1), and $N_{\mathrm{antitag,rare}}^{\mathrm{MC},0\ell}$ denotes the number of rare background events, such as diboson and triboson events, expected from simulation.

The predictions of the top quark backgrounds and 0-res backgrounds are taken from Eqs. (1) and (2), while the prediction of the rare backgrounds is taken from simulation. These predictions are produced in each $p_{\mathrm{T}}^{\mathrm{miss}}$ bin and in each SR independently. Each transfer factor is derived separately for each $p_{\mathrm{T}}^{\mathrm{miss}}$ bin except for $\mathcal{R}_{0\ell/1\ell}$, whose values above $p_{\mathrm{T}}^{\mathrm{miss}} > 450$ (400) GeV are averaged in the W and H (WH) SRs.

The predictions of the SM backgrounds are tested in data using an orthogonal VR in which exactly one AK8 jet is required. This VR is used to test the simulation-derived transfer factors, misidentification scale factors, and simulation-based contamination terms in the CRs. Within the VR, two pseudo-SRs are defined in which the AK8 jet is W tagged or $\mathrm{b\bar{b}}$ tagged, respectively. For each pseudo-SR, a 0ℓ antitag CR and 1ℓ tag and antitag CRs are defined for the

background estimation. All transfer factors are rederived in the VR phase space. Predictions and observations in the pseudo-SRs are found to be statistically compatible.

6 Systematic uncertainties

For all SRs and CRs, the expected rate of signal and backgrounds is adjusted for known differences between data and simulation in the jet tagging rates (using the b, $\mathrm{b\overline{b}}$, W, and V taggers), lepton identification rates, and trigger efficiencies. Additional corrections are applied to the predicted signal yields to account for known differences between the GEANT4-based CMS detector simulation and the CMS fast simulation in the AK8 jet mass, W tagging, V tagging, $\mathrm{b\overline{b}}$ tagging, b tagging, and $p_{\mathrm{T}}^{\mathrm{miss}}$. Uncertainties associated with the determination of these correction factors are propagated to the final yield estimates, as is the uncertainty in the integrated luminosity [94–96]. Uncertainties related to the determination of the trigger efficiency are dominated by the limited size of the data sets in which we measure the trigger efficiency at high $p_{\mathrm{T}}^{\mathrm{miss}}$ and by the differences between the efficiencies determined using two classes of events, namely events with one electron and events with one muon, at low $p_{\mathrm{T}}^{\mathrm{miss}}$. Uncertainties related to the corrections to the rates of jet misidentification are due to the limited size of our dilepton data sets. Uncertainties associated with the lepton identification efficiency corrections and jet tagging rate corrections are detailed in Refs. [87, 88] and [49, 86], respectively. In this analysis, the W tagger is used to identify $\mathrm{W}(\mathrm{q\overline{q}}')$ decays, but some signal events with ZH and large $p_{\mathrm{T}}^{\mathrm{miss}}$ in the higgsino-like NLSP scenario enter the b-tag WH or W SRs when $\mathrm{Z}(\mathrm{q\overline{q}})$ decays are selected by the W tagger. The W tagger efficiency is lower for $\mathrm{Z}(\mathrm{q\overline{q}})$ decays than for $\mathrm{W}(\mathrm{q\overline{q}}')$ decays by 20–40% in simulation, but its performance is calibrated only for $\mathrm{W}(\mathrm{q\overline{q}}')$ decays and not for $\mathrm{Z}(\mathrm{q\overline{q}})$ decays in data. Therefore, additional uncertainties, corresponding to half the W tagger efficiency differences between $\mathrm{W}(\mathrm{q\overline{q}}')$ and $\mathrm{Z}(\mathrm{q\overline{q}})$ decays in simulation, are applied when ZH signal events enter the b-tag WH or W SRs, but they do not affect our results significantly. The corrections to the jet tagging rates in the b-veto SR and CRs derived from the VRs described in Section 5.1 are treated as systematic uncertainties, and are referred to as the "nonclosure" uncertainties. Additional uncertainties associated with the choice of the renormalization and factorization scales μ_{R} and μ_{F} were assessed by varying them independently up and down by a factor of 2, ignoring the case in which one parameter is scaled up while the other is scaled down. Several other sources of uncertainties related to jet energy scale and resolution, $p_{\mathrm{T}}^{\mathrm{miss}}$ modeling, effects of pileup, and choice of PDF were studied, which collectively have less than 2% impact on our predictions. The statistical treatment of the systematic uncertainties is described in Section 7. Summaries of the dominant systematic uncertainties and their impacts on the yields of the various sources of background and the signal are presented in Table 3.

Among these uncertainties, except for those from the sizes of the CR data and MC samples, the two leading systematic uncertainties that affect the 95% confidence level (CL) upper limits on the signal production cross sections discussed in the next section are the W-tag nonclosure and W-tag correction uncertainties. These degrade the cross section upper limits by up to about 15 and 10%, respectively, depending on the signal model and the SUSY particle masses. The others have much smaller impacts.

7 Results

We perform simultaneous fits using a statistical model of our signal and SM background predictions. The likelihood used for the fits is a product of Poisson distributions, one for each $p_{\mathrm{T}}^{\mathrm{miss}}$

Table 3: The dominant systematic uncertainties and their effects on event yields (in %) in various SRs. For the 0- and 1-res backgrounds in the b-veto SR, uncertainties are presented separately depending on the CR region used for the estimation. A dash (—) indicates that the source of uncertainty is not applicable.

	b veto				b tag			
Source	0- and 1-res bkg.		Rare	Signal	Top quark	0-res	Rare	Signal
	0-tag CR	1-tag CR						
Integr. luminosity	—	—	1.6	1.6	—	—	1.6	1.6
CR data size	6–71	5–50	—	—	3–100	2–35	—	—
MC sample size	8–25	8–30	14–24	2–5	2–28	3–40	4–27	2–5
μ_R and μ_F	1.2	0.4	8	<5	2–10	0.5	11	<5
Trigger efficiency	—	—	2–3	2–3	—	—	2–3	2–3
b-tag correction	<1	<1	<1	1	1	<3	<3	2–3
$b\bar{b}$-tag correction	—	—	—	—	—	4	2–7	4
W-tag correction	12–28	6–22	11–15	15	1	9	7	9
V-tag correction	7–15	2–10	1–4	2	—	—	—	—
W-tag nonclosure	3–48	3–48	—	—	—	—	—	—
V-tag nonclosure	1–27	—	—	—	—	—	—	—
Fast simulation	—	—	—	5	—	—	—	8

bin of each SR and CR. The systematic uncertainties are included in the likelihood as nuisance parameters with log-normal constraints [97], with the exception of the systematic uncertainties related to the finite size of the simulation, which use the method described in Ref. [98]. This fitting procedure further constrains the predictions and the uncertainties in the predictions. The yields of the SM backgrounds, determined from the fit applied only to the CRs under the background-only hypothesis, are shown along with the predicted yields of the signals and the observations in Fig. 3. No statistically significant excess of events is observed in the data with respect to the SM background predictions.

We place 95% CL upper limits on the production cross section of either pairs of charginos or a chargino and a neutralino together. The limits are computed based on a binned likelihood fit to the data in all of the b-veto and b-tag SRs and CRs, which takes into account the predicted background and signal yields. A test statistic is used in conjunction with the CL_s criterion [99, 100] to set upper limits. The test statistic is the profile likelihood ratio, modified for upper limits [101]. We compute limits using the asymptotic approximation [102].

By comparing the upper limits on the production cross sections to the cross sections predicted for chargino-pair production and for chargino-neutralino production, 95% CL mass exclusion contours are derived. The 95% CL mass exclusion contours within the NLSP-LSP mass plane are shown in Fig. 4 (upper left and upper right) for the TChiWW and TChiWZ models. We exclude NLSP masses between 290 and 670 GeV assuming a pair of charginos are produced and result in a pair of W bosons and a pair of light LSPs. For low-mass LSPs, we exclude NLSP masses between 230 and 760 GeV assuming chargino-neutralino production resulting in W and Z bosons and a large p_T^{miss}. In the case of chargino-neutralino production with a W boson and a Higgs boson, for low-mass LSPs we exclude NLSP masses between 240 and 970 GeV. Figure 4 (lower) shows limits in the NLSP-LSP mass plane for the TChiWH model. The observed limits are slightly weaker than the expected limits because a few intermediate p_T^{miss} bins of the WH SR contain more observed events than expected.

We also consider models including both $\widetilde{\chi}_1^{\pm}\widetilde{\chi}_1^{\mp}$ and $\widetilde{\chi}_1^{\pm}\widetilde{\chi}_2^0$ production where the $\widetilde{\chi}_1^{\pm}$ and $\widetilde{\chi}_2^0$ are the mass-degenerate wino-like NLSPs. The expected and observed mass exclusions are

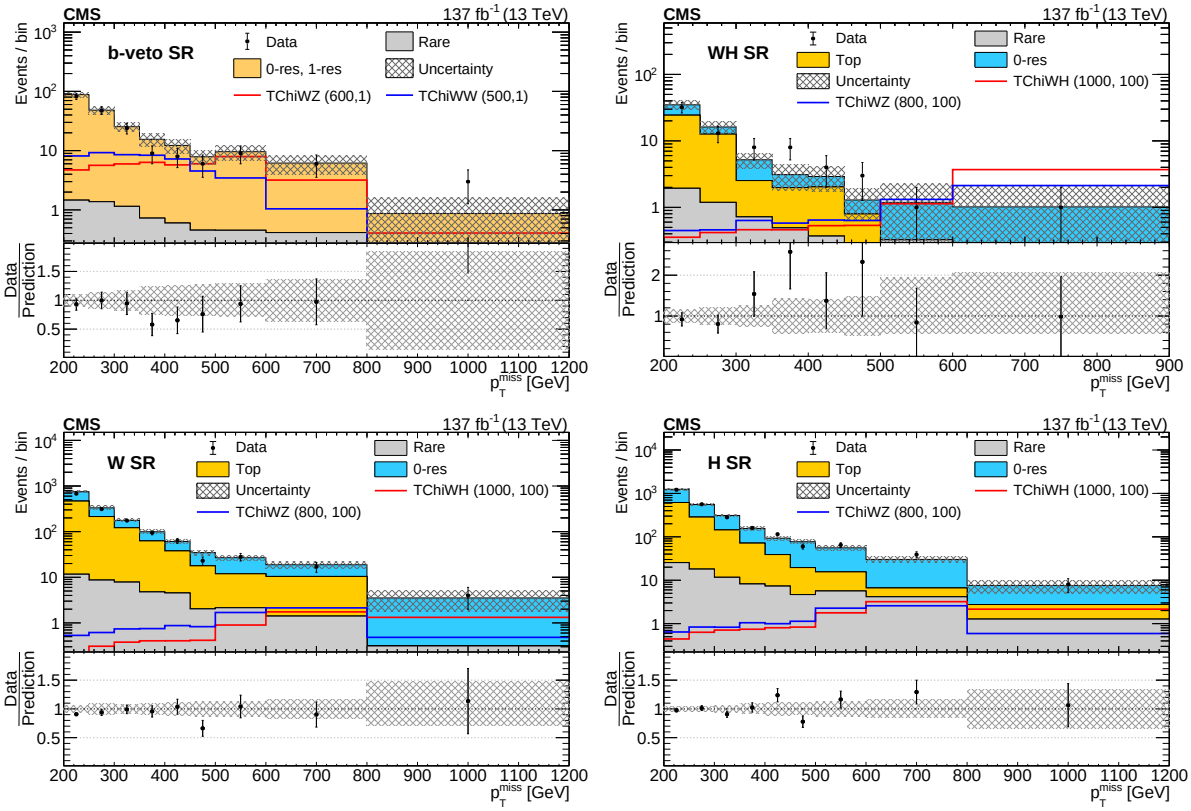

Figure 3: SM background prediction vs. observation in the b-veto SR (upper left), the WH SR (upper right), the W SR (lower left), and the H SR (lower right). The filled stacked histograms show the SM background predictions from the fit to the data in the CRs under the background-only hypothesis. The superimposed open histograms show the expectations for selected signal models, which are denoted in the legend by the name of the model followed by the assumed masses of the NLSP and LSP in GeV. The observed event yields are indicated by black markers. The hatched gray band corresponds to the total uncertainty in the prediction.

presented in Fig. 5 (left). For the scenarios of $\widetilde{\chi}_2^0 \to \mathrm{Z}\widetilde{\chi}_1^0$ or $\widetilde{\chi}_2^0 \to \mathrm{H}\widetilde{\chi}_1^0$, wino-like NLSP masses up to 870 and 960 GeV are excluded, respectively, while exclusions up to 1010 and 1110 GeV are expected under the background-only hypothesis.

Figure 5 (right) shows the results for the mass-degenerate higgsino-like NLSP scenario including $\widetilde{\chi}_1^\pm\widetilde{\chi}_1^\mp$, $\widetilde{\chi}_1^\pm\widetilde{\chi}_2^0$, $\widetilde{\chi}_1^\pm\widetilde{\chi}_3^0$, and $\widetilde{\chi}_2^0\widetilde{\chi}_3^0$ production. In this scenario, higgsino-like NLSP masses from 300 to 650 GeV are excluded. The expected exclusion reaches from 320 to 810 GeV. The observed exclusion is weaker than expected mainly because of a modest excess in the data over the background prediction in the $300 < p_\mathrm{T}^\mathrm{miss} < 500$ GeV region of the WH SR.

8 Summary

A search is presented for signatures of electroweak production of charginos and neutralinos in fully hadronic final states. The charginos are assumed to decay to the W boson and the lightest neutralino $\widetilde{\chi}_1^0$, and the heavier neutralinos ($\widetilde{\chi}_2^0$ and $\widetilde{\chi}_3^0$) are assumed to decay to either the Z or Higgs boson (H) and $\widetilde{\chi}_1^0$. The decay products of W, Z, or Higgs bosons are clustered into large-radius jets. These jets are categorized based on their mass and a collection of novel jet-tagging algorithms based on deep neural networks. Four search regions, three that require b tags and one that excludes b tags, are constructed to look for chargino- and neutralino-mediated pro-

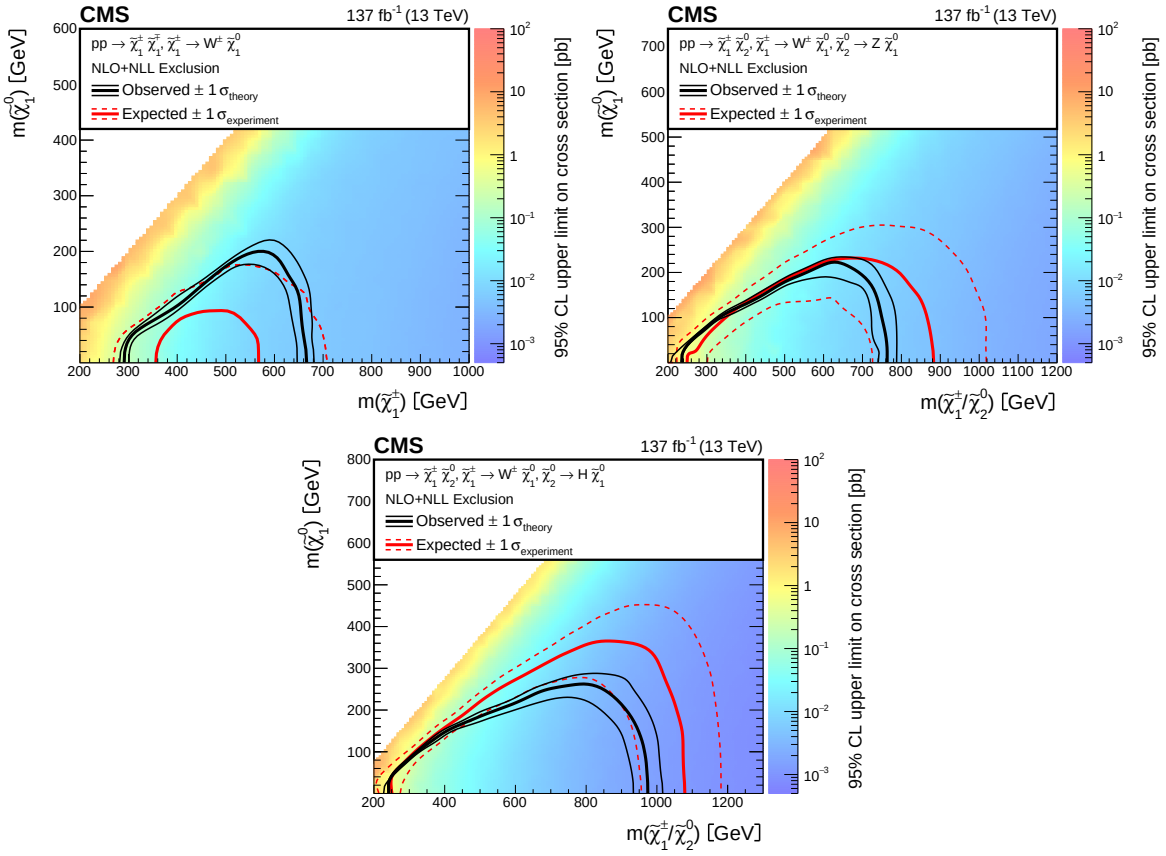

Figure 4: The 95% CL upper limits on the production cross sections for $\widetilde{\chi}_1^{\pm}\widetilde{\chi}_1^{\mp}$ assuming that each $\widetilde{\chi}_1^{\pm}$ decays to a W boson and $\widetilde{\chi}_1^0$ (upper left, the TChiWW model) and $\widetilde{\chi}_1^{\pm}\widetilde{\chi}_2^0$ production assuming that the $\widetilde{\chi}_1^{\pm}$ decays to a W boson and $\widetilde{\chi}_1^0$ and that the $\widetilde{\chi}_2^0$ decays to a Z boson and $\widetilde{\chi}_1^0$ (upper right, the TChiWZ model) or that the $\widetilde{\chi}_2^0$ decays to a Higgs boson and $\widetilde{\chi}_1^0$ (lower, the TChiWH model). The black curves represent the observed exclusion contour and the change in this contour due to variation of these cross sections within their theoretical uncertainties (σ_{theory}). The red curves indicate the mean expected exclusion contour and the region containing 68% ($\pm 1\,\sigma_{\text{experiment}}$) of the expected exclusion limits under the background-only hypothesis. The mass exclusion limits are computed assuming wino-like cross sections.

duction of a pair of bosons, WW, WZ, or WH, together with a large transverse momentum imbalance. We consider simplified models in which the charginos $\widetilde{\chi}_1^{\pm}$ and the next-to-lightest neutralino $\widetilde{\chi}_2^0$ are assumed to be the mass-degenerate next-to-lightest supersymmetric particles (NLSPs). The lightest neutralino $\widetilde{\chi}_1^0$ is assumed to be bino-like and to be the lightest supersymmetric particle (LSP). No statistically significant excess of events is observed in the data with respect to the expectation from the standard model.

Using wino-like pair production cross sections, 95% confidence level mass exclusions are derived. For signals with WW, WZ, or WH boson pairs, the NLSP mass exclusion limit for low-mass LSPs extends up to 670, 760, and 970 GeV, respectively. When we consider models including both wino-like NLSP $\widetilde{\chi}_1^{\pm}\widetilde{\chi}_2^0$ and $\widetilde{\chi}_1^{\pm}\widetilde{\chi}_1^{\mp}$ production under the assumption that either $\widetilde{\chi}_2^0 \to Z\widetilde{\chi}_1^0$ or $\widetilde{\chi}_2^0 \to H\widetilde{\chi}_1^0$, the NLSP mass exclusion extends up to 870 and 960 GeV, respectively. Alternatively, with higgsino-like NLSPs $\widetilde{\chi}_1^{\pm}$, $\widetilde{\chi}_2^0$, and $\widetilde{\chi}_3^0$, the higgsino masses from 300 to 650 GeV are excluded for low-mass LSPs. These mass exclusions significantly improve on those achieved by searches using leptonic probes of SUSY for high NLSP masses.

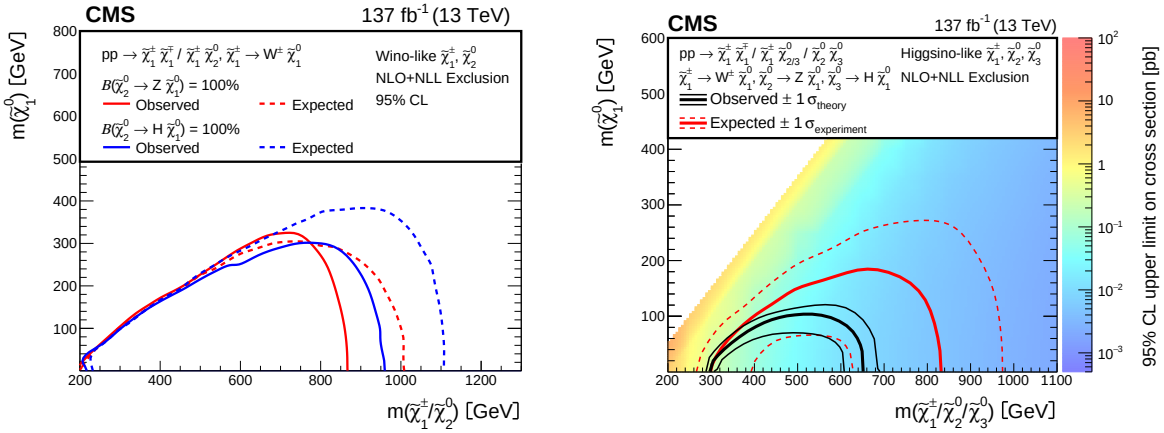

Figure 5: Expected and observed 95% CL exclusion for mass-degenerate wino-like $\widetilde{\chi}_1^{\pm}\widetilde{\chi}_1^{\mp}$ and $\widetilde{\chi}_1^{\pm}\widetilde{\chi}_2^0$ production (left) and higgsino-like $\widetilde{\chi}_1^{\pm}\widetilde{\chi}_1^{\mp}$, $\widetilde{\chi}_1^{\pm}\widetilde{\chi}_2^0$, $\widetilde{\chi}_1^{\pm}\widetilde{\chi}_3^0$, and $\widetilde{\chi}_2^0\widetilde{\chi}_3^0$ production (right) as functions of the NLSP and LSP masses. The $\widetilde{\chi}_1^{\pm}$, $\widetilde{\chi}_2^0$, and $\widetilde{\chi}_3^0$ are considered to be mass degenerate. For the higgsino-like case (right), the 95% CL upper limits on the production cross sections are also shown, but they are not shown for the wino-like case (left) because there are two distinct sets of limits depending on the chargino decay mode.

References

[1] P. Ramond, "Dual theory for free fermions", *Phys. Rev. D* **3** (1971) 2415, doi:10.1103/PhysRevD.3.2415.

[2] Y. A. Golfand and E. P. Likhtman, "Extension of the algebra of Poincaré group generators and violation of P invariance", *JETP Lett.* **13** (1971) 323.

[3] A. Neveu and J. H. Schwarz, "Factorizable dual model of pions", *Nucl. Phys. B* **31** (1971) 86, doi:10.1016/0550-3213(71)90448-2.

[4] D. V. Volkov and V. P. Akulov, "Possible universal neutrino interaction", *JETP Lett.* **16** (1972) 438.

[5] J. Wess and B. Zumino, "A Lagrangian model invariant under supergauge transformations", *Phys. Lett. B* **49** (1974) 52, doi:10.1016/0370-2693(74)90578-4.

[6] J. Wess and B. Zumino, "Supergauge transformations in four dimensions", *Nucl. Phys. B* **70** (1974) 39, doi:10.1016/0550-3213(74)90355-1.

[7] P. Fayet, "Supergauge invariant extension of the Higgs mechanism and a model for the electron and its neutrino", *Nucl. Phys. B* **90** (1975) 104, doi:10.1016/0550-3213(75)90636-7.

[8] P. Fayet and S. Ferrara, "Supersymmetry", *Phys. Rept.* **32** (1977) 249, doi:10.1016/0370-1573(77)90066-7.

[9] H. P. Nilles, "Supersymmetry, supergravity and particle physics", *Phys. Rept.* **110** (1984) 1, doi:10.1016/0370-1573(84)90008-5.

[10] S. P. Martin, "A supersymmetry primer", *Adv. Ser. Direct. High Energy Phys.* **21** (2010) 1, doi:10.1142/9789814307505_0001, arXiv:hep-ph/9709356.

[11] M. Papucci, J. T. Ruderman, and A. Weiler, "Natural SUSY endures", *JHEP* **09** (2012) 035, doi:10.1007/JHEP09(2012)035, arXiv:1110.6926.

[12] H. Baer et al., "Natural SUSY with a bino- or wino-like LSP", *Phys. Rev. D* **91** (2015) 075005, doi:10.1103/PhysRevD.91.075005, arXiv:1501.06357.

[13] H. Baer, V. Barger, N. Nagata, and M. Savoy, "Phenomenological profile of top squarks from natural supersymmetry at the LHC", *Phys. Rev. D* **95** (2017) 055012, doi:10.1103/PhysRevD.95.055012, arXiv:1611.08511. [Erratum: doi:10.1103/PhysRevD.103.059902].

[14] ATLAS Collaboration, "Search for bottom-squark pair production with the ATLAS detector in final states containing Higgs bosons, b-jets and missing transverse momentum", *JHEP* **12** (2019) 060, doi:10.1007/JHEP12(2019)060, arXiv:1908.03122.

[15] ATLAS Collaboration, "Search for a scalar partner of the top quark in the all-hadronic $t\bar{t}$ plus missing transverse momentum final state at $\sqrt{s} = 13$ TeV with the ATLAS detector", *Eur. Phys. J. C* **80** (2020) 737, doi:10.1140/epjc/s10052-020-8102-8, arXiv:2004.14060.

[16] ATLAS Collaboration, "Search for squarks and gluinos in final states with jets and missing transverse momentum using 139 fb^{-1} of $\sqrt{s} = 13$ TeV pp collision data with the ATLAS detector", *JHEP* **02** (2021) 143, doi:10.1007/JHEP02(2021)143, arXiv:2010.14293.

[17] ATLAS Collaboration, "Search for new phenomena with top quark pairs in final states with one lepton, jets, and missing transverse momentum in pp collisions at $\sqrt{s} = 13$ TeV with the ATLAS detector", *JHEP* **04** (2021) 174, doi:10.1007/JHEP04(2021)174, arXiv:2012.03799.

[18] ATLAS Collaboration, "Search for squarks and gluinos in final states with one isolated lepton, jets, and missing transverse momentum at $\sqrt{s} = 13$ TeV with the ATLAS detector", *Eur. Phys. J. C* **81** (2021) 600, doi:10.1140/epjc/s10052-021-09344-w, arXiv:2101.01629.

[19] ATLAS Collaboration, "Search for new phenomena in final states with b-jets and missing transverse momentum in $\sqrt{s} = 13$ TeV pp collisions with the ATLAS detector", *JHEP* **05** (2021) 093, doi:10.1007/JHEP05(2021)093, arXiv:2101.12527.

[20] ATLAS Collaboration, "Search for new phenomena in events with two opposite-charge leptons, jets and missing transverse momentum in pp collisions at $\sqrt{s} = 13$ TeV with the ATLAS detector", *JHEP* **04** (2021) 165, doi:10.1007/JHEP04(2021)165, arXiv:2102.01444.

[21] ATLAS Collaboration, "Search for bottom-squark pair production in pp collision events at $\sqrt{s} = 13$ TeV with hadronically decaying τ-leptons, b-jets and missing transverse momentum using the ATLAS detector", *Phys. Rev. D* **104** (2021) 032014, doi:10.1103/PhysRevD.104.032014, arXiv:2103.08189.

[22] CMS Collaboration, "Search for supersymmetry in proton-proton collisions at 13 TeV in final states with jets and missing transverse momentum", *JHEP* **10** (2019) 244, doi:10.1007/JHEP10(2019)244, arXiv:1908.04722.

[23] CMS Collaboration, "Searches for physics beyond the standard model with the M_{T2} variable in hadronic final states with and without disappearing tracks in proton-proton collisions at $\sqrt{s} = 13$ TeV", *Eur. Phys. J. C* **80** (2020) 3, doi:10.1140/epjc/s10052-019-7493-x, arXiv:1909.03460.

[24] CMS Collaboration, "Search for supersymmetry in pp collisions at $\sqrt{s} = 13$ TeV with 137 fb^{-1} in final states with a single lepton using the sum of masses of large-radius jets", *Phys. Rev. D* **101** (2020) 052010, doi:10.1103/PhysRevD.101.052010, arXiv:1911.07558.

[25] CMS Collaboration, "Search for direct top squark pair production in events with one lepton, jets, and missing transverse momentum at 13 TeV with the CMS experiment", *JHEP* **05** (2020) 032, doi:10.1007/JHEP05(2020)032, arXiv:1912.08887.

[26] CMS Collaboration, "Search for top squark pair production using dilepton final states in pp collision data collected at $\sqrt{s} = 13$ TeV", *Eur. Phys. J. C* **81** (2021) 3, doi:10.1140/epjc/s10052-020-08701-5, arXiv:2008.05936.

[27] CMS Collaboration, "Search for top squark production in fully hadronic final states in proton-proton collisions at $\sqrt{s} = 13$ TeV", *Phys. Rev. D* **104** (2021) 052001, doi:10.1103/PhysRevD.104.052001, arXiv:2103.01290.

[28] CMS Collaboration, "Combined searches for the production of supersymmetric top quark partners in proton-proton collisions at $\sqrt{s} = 13$ TeV", *Eur. Phys. J. C* **81** (2021) 970, doi:10.1140/epjc/s10052-021-09721-5, arXiv:2107.10892.

[29] G. R. Farrar and P. Fayet, "Phenomenology of the production, decay, and detection of new hadronic states associated with supersymmetry", *Phys. Lett. B* **76** (1978) 575, doi:10.1016/0370-2693(78)90858-4.

[30] ATLAS Collaboration, "Search for electroweak production of supersymmetric particles in final states with two or three leptons at $\sqrt{s} = 13$ TeV with the ATLAS detector", *Eur. Phys. J. C* **78** (2018) 995, doi:10.1140/epjc/s10052-018-6423-7, arXiv:1803.02762.

[31] ATLAS Collaboration, "Search for chargino-neutralino production using recursive jigsaw reconstruction in final states with two or three charged leptons in proton-proton collisions at $\sqrt{s} = 13$ TeV with the ATLAS detector", *Phys. Rev. D* **98** (2018) 092012, doi:10.1103/PhysRevD.98.092012, arXiv:1806.02293.

[32] ATLAS Collaboration, "Search for chargino and neutralino production in final states with a Higgs boson and missing transverse momentum at $\sqrt{s} = 13$ TeV with the ATLAS detector", *Phys. Rev. D* **100** (2019) 012006, doi:10.1103/PhysRevD.100.012006, arXiv:1812.09432.

[33] ATLAS Collaboration, "Search for electroweak production of charginos and sleptons decaying into final states with two leptons and missing transverse momentum in $\sqrt{s} = 13$ TeV pp collisions using the ATLAS detector", *Eur. Phys. J. C* **80** (2020) 123, doi:10.1140/epjc/s10052-019-7594-6, arXiv:1908.08215.

[34] ATLAS Collaboration, "Search for direct production of electroweakinos in final states with one lepton, missing transverse momentum and a Higgs boson decaying into two b-jets in pp collisions at $\sqrt{s} = 13$ TeV with the ATLAS detector", *Eur. Phys. J. C* **80** (2020) 691, doi:10.1140/epjc/s10052-020-8050-3, arXiv:1909.09226.

[35] ATLAS Collaboration, "Search for chargino-neutralino production with mass splittings near the electroweak scale in three-lepton final states in $\sqrt{s} = 13$ TeV pp collisions with the ATLAS detector", *Phys. Rev. D* **101** (2020) 072001, doi:10.1103/PhysRevD.101.072001, arXiv:1912.08479.

[36] ATLAS Collaboration, "Search for chargino–neutralino pair production in final states with three leptons and missing transverse momentum in $\sqrt{s} = 13$ TeV pp collisions with the ATLAS detector", *Eur. Phys. J. C* **81** (2021) 1118, doi:10.1140/epjc/s10052-021-09749-7, arXiv:2106.01676.

[37] ATLAS Collaboration, "Search for charginos and neutralinos in final states with two boosted hadronically decaying bosons and missing transverse momentum in pp collisions at $\sqrt{s} = 13$ TeV with the ATLAS detector", *Phys. Rev. D* **104** (2021) 112010, doi:10.1103/PhysRevD.104.112010, arXiv:2108.07586.

[38] ATLAS Collaboration, "Searches for new phenomena in events with two leptons, jets, and missing transverse momentum in 139 fb^{-1} of $\sqrt{s} = 13$ TeV pp collisions with the ATLAS detector", 2022. arXiv:2204.13072. Submitted to *Eur. Phys. J. C*.

[39] CMS Collaboration, "Search for electroweak production of charginos and neutralinos in WH events in proton-proton collisions at $\sqrt{s} = 13$ TeV", *JHEP* **11** (2017) 029, doi:10.1007/JHEP11(2017)029, arXiv:1706.09933.

[40] CMS Collaboration, "Search for electroweak production of charginos and neutralinos in multilepton final states in proton-proton collisions at $\sqrt{s} = 13$ TeV", *JHEP* **03** (2018) 166, doi:10.1007/JHEP03(2018)166, arXiv:1709.05406.

[41] CMS Collaboration, "Combined search for electroweak production of charginos and neutralinos in proton-proton collisions at $\sqrt{s} = 13$ TeV", *JHEP* **03** (2018) 160, doi:10.1007/JHEP03(2018)160, arXiv:1801.03957.

[42] CMS Collaboration, "Searches for pair production of charginos and top squarks in final states with two oppositely charged leptons in proton-proton collisions at $\sqrt{s} = 13$ TeV", *JHEP* **11** (2018) 079, doi:10.1007/JHEP11(2018)079, arXiv:1807.07799.

[43] CMS Collaboration, "Search for supersymmetry in final states with two oppositely charged same-flavor leptons and missing transverse momentum in proton-proton collisions at $\sqrt{s} = 13$ TeV", *JHEP* **04** (2021) 123, doi:10.1007/JHEP04(2021)123, arXiv:2012.08600.

[44] CMS Collaboration, "Search for electroweak production of charginos and neutralinos in proton-proton collisions at $\sqrt{s} = 13$ TeV", *JHEP* **04** (2022) 147, doi:10.1007/JHEP04(2022)147, arXiv:2106.14246.

[45] CMS Collaboration, "Search for chargino-neutralino production in events with Higgs and W bosons using 137 fb^{-1} of proton-proton collisions at $\sqrt{s} = 13$ TeV", *JHEP* **10** (2021) 045, doi:10.1007/JHEP10(2021)045, arXiv:2107.12553.

[46] ATLAS Collaboration, "Search for pair production of higgsinos in final states with at least three b-tagged jets in $\sqrt{s} = 13$ TeV pp collisions using the ATLAS detector", *Phys. Rev. D* **98** (2018) 092002, doi:10.1103/PhysRevD.98.092002, arXiv:1806.04030.

[47] CMS Collaboration, "Searches for electroweak neutralino and chargino production in channels with Higgs, Z, and W bosons in pp collisions at 8 TeV", *Phys. Rev. D* **90** (2014) 092007, doi:10.1103/PhysRevD.90.092007, arXiv:1409.3168.

[48] CMS Collaboration, "Search for higgsino pair production in pp collisions at $\sqrt{s}$ = 13 TeV in final states with large missing transverse momentum and two Higgs bosons decaying via $H \to b\bar{b}$", *Phys. Rev. D* **97** (2018) 032007, doi:10.1103/PhysRevD.97.032007, arXiv:1709.04896.

[49] CMS Collaboration, "Identification of heavy, energetic, hadronically decaying particles using machine-learning techniques", *JINST* **15** (2020) P06005, doi:10.1088/1748-0221/15/06/P06005, arXiv:2004.08262.

[50] HEPData record for this analysis, 2022. doi:10.17182/hepdata.127766.

[51] J. Alwall et al., "The automated computation of tree-level and next-to-leading order differential cross sections, and their matching to parton shower simulations", *JHEP* **07** (2014) 079, doi:10.1007/JHEP07(2014)079, arXiv:1405.0301.

[52] P. Nason, "A new method for combining NLO QCD with shower Monte Carlo algorithms", *JHEP* **11** (2004) 040, doi:10.1088/1126-6708/2004/11/040, arXiv:hep-ph/0409146.

[53] S. Frixione, P. Nason, and C. Oleari, "Matching NLO QCD computations with parton shower simulations: the POWHEG method", *JHEP* **11** (2007) 070, doi:10.1088/1126-6708/2007/11/070, arXiv:0709.2092.

[54] S. Alioli, P. Nason, C. Oleari, and E. Re, "A general framework for implementing NLO calculations in shower Monte Carlo programs: the POWHEG BOX", *JHEP* **06** (2010) 043, doi:10.1007/JHEP06(2010)043, arXiv:1002.2581.

[55] S. Alioli, P. Nason, C. Oleari, and E. Re, "NLO single-top production matched with shower in POWHEG: s- and t-channel contributions", *JHEP* **09** (2009) 111, doi:10.1088/1126-6708/2009/09/111, arXiv:0907.4076. [Erratum: doi:10.1007/JHEP02(2010)011].

[56] E. Re, "Single-top Wt-channel production matched with parton showers using the POWHEG method", *Eur. Phys. J. C* **71** (2011) 1547, doi:10.1140/epjc/s10052-011-1547-z, arXiv:1009.2450.

[57] T. Melia, P. Nason, R. Röntsch, and G. Zanderighi, "W^+W^-, WZ and ZZ production in the POWHEG BOX", *JHEP* **11** (2011) 078, doi:10.1007/JHEP11(2011)078, arXiv:1107.5051.

[58] P. Nason and G. Zanderighi, "W^+W^-, WZ and ZZ production in the POWHEG-BOX-V2", *Eur. Phys. J. C* **74** (2014) 2702, doi:10.1140/epjc/s10052-013-2702-5, arXiv:1311.1365.

[59] H. B. Hartanto, B. Jäger, L. Reina, and D. Wackeroth, "Higgs boson production in association with top quarks in the POWHEG BOX", *Phys. Rev. D* **91** (2015) 094003, doi:10.1103/PhysRevD.91.094003, arXiv:1501.04498.

[60] NNPDF Collaboration, "Parton distributions for the LHC run II", *JHEP* **04** (2015) 040, doi:10.1007/JHEP04(2015)040, arXiv:1410.8849.

[61] NNPDF Collaboration, "Parton distributions from high-precision collider data", *Eur. Phys. J. C* **77** (2017) 663, doi:10.1140/epjc/s10052-017-5199-5, arXiv:1706.00428.

[62] T. Sjöstrand et al., "An introduction to PYTHIA 8.2", *Comput. Phys. Commun.* **191** (2015) 159, doi:10.1016/j.cpc.2015.01.024, arXiv:1410.3012.

[63] CMS Collaboration, "Event generator tunes obtained from underlying event and multiparton scattering measurements", *Eur. Phys. J. C* **76** (2016) 155, doi:10.1140/epjc/s10052-016-3988-x, arXiv:1512.00815.

[64] CMS Collaboration, "Extraction and validation of a new set of CMS PYTHIA8 tunes from underlying-event measurements", *Eur. Phys. J. C* **80** (2020) 4, doi:10.1140/epjc/s10052-019-7499-4, arXiv:1903.12179.

[65] GEANT4 Collaboration, "GEANT4 — a simulation toolkit", *Nucl. Instrum. Meth. A* **506** (2003) 250, doi:10.1016/S0168-9002(03)01368-8.

[66] S. Abdullin et al., "The fast simulation of the CMS detector at LHC", *J. Phys. Conf. Ser.* **331** (2011) 032049, doi:10.1088/1742-6596/331/3/032049.

[67] A. Giammanco, "The fast simulation of the CMS experiment", *J. Phys. Conf. Ser.* **513** (2014) 022012, doi:10.1088/1742-6596/513/2/022012.

[68] B. Fuks, M. Klasen, D. R. Lamprea, and M. Rothering, "Gaugino production in proton-proton collisions at a center-of-mass energy of 8 TeV", *JHEP* **10** (2012) 081, doi:10.1007/JHEP10(2012)081, arXiv:1207.2159.

[69] B. Fuks, M. Klasen, D. R. Lamprea, and M. Rothering, "Precision predictions for electroweak superpartner production at hadron colliders with RESUMMINO", *Eur. Phys. J. C* **73** (2013) 2480, doi:10.1140/epjc/s10052-013-2480-0, arXiv:1304.0790.

[70] N. Arkani-Hamed et al., "MARMOSET: the path from LHC data to the new standard model via on-shell effective theories", 2007. arXiv:hep-ph/0703088..

[71] J. Alwall, P. C. Schuster, and N. Toro, "Simplified models for a first characterization of new physics at the LHC", *Phys. Rev. D* **79** (2009) 075020, doi:10.1103/PhysRevD.79.075020, arXiv:0810.3921.

[72] J. Alwall, M.-P. Le, M. Lisanti, and J. G. Wacker, "Model-independent jets plus missing energy searches", *Phys. Rev. D* **79** (2009) 015005, doi:10.1103/PhysRevD.79.015005, arXiv:0809.3264.

[73] D. Alves et al., "Simplified models for LHC new physics searches", *J. Phys. G* **39** (2012) 105005, doi:10.1088/0954-3899/39/10/105005, arXiv:1105.2838.

[74] CMS Collaboration, "Interpretation of searches for supersymmetry with simplified models", *Phys. Rev. D* **88** (2013) 052017, doi:10.1103/PhysRevD.88.052017, arXiv:1301.2175.

[75] T. Han, S. Padhi, and S. Su, "Electroweakinos in the light of the Higgs boson", *Phys. Rev. D* **88** (2013) 115010, doi:10.1103/PhysRevD.88.115010, arXiv:1309.5966.

[76] P. Agrawal, J. Fan, M. Reece, and W. Xue, "Deciphering the MSSM Higgs mass at future hadron colliders", *JHEP* **06** (2017) 027, doi:10.1007/JHEP06(2017)027, arXiv:1702.05484.

[77] CMS Collaboration, "The CMS experiment at the CERN LHC", *JINST* **3** (2008) S08004, doi:10.1088/1748-0221/3/08/S08004.

[78] CMS Collaboration, "Particle-flow reconstruction and global event description with the CMS detector", *JINST* **12** (2017) P10003, doi:10.1088/1748-0221/12/10/P10003, arXiv:1706.04965.

[79] M. Cacciari, G. P. Salam, and G. Soyez, "The anti-k_{T} jet clustering algorithm", *JHEP* **04** (2008) 063, doi:10.1088/1126-6708/2008/04/063, arXiv:0802.1189.

[80] M. Cacciari, G. P. Salam, and G. Soyez, "FastJet user manual", *Eur. Phys. J. C* **72** (2012) 1896, doi:10.1140/epjc/s10052-012-1896-2, arXiv:1111.6097.

[81] CMS Collaboration, "Pileup mitigation at CMS in 13 TeV data", *JINST* **15** (2020) P09018, doi:10.1088/1748-0221/15/09/p09018, arXiv:2003.00503.

[82] D. Bertolini, P. Harris, M. Low, and N. Tran, "Pileup per particle identification", *JHEP* **10** (2014) 059, doi:10.1007/JHEP10(2014)059, arXiv:1407.6013.

[83] CMS Collaboration, "Jet energy scale and resolution in the CMS experiment in pp collisions at 8 TeV", *JINST* **12** (2017) P02014, doi:10.1088/1748-0221/12/02/P02014, arXiv:1607.03663.

[84] A. J. Larkoski, S. Marzani, G. Soyez, and J. Thaler, "Soft drop", *JHEP* **05** (2014) 146, doi:10.1007/JHEP05(2014)146, arXiv:1402.2657.

[85] CMS Collaboration, "Performance of missing transverse momentum reconstruction in proton-proton collisions at $\sqrt{s} = 13$ TeV using the CMS detector", *JINST* **14** (2019) P07004, doi:10.1088/1748-0221/14/07/P07004, arXiv:1903.06078.

[86] CMS Collaboration, "Identification of heavy-flavour jets with the CMS detector in pp collisions at 13 TeV", *JINST* **13** (2018) P05011, doi:10.1088/1748-0221/13/05/P05011, arXiv:1712.07158.

[87] CMS Collaboration, "Performance of electron reconstruction and selection with the CMS detector in proton-proton collisions at $\sqrt{s} = 8$ TeV", *JINST* **10** (2015) P06005, doi:10.1088/1748-0221/10/06/P06005, arXiv:1502.02701.

[88] CMS Collaboration, "Performance of the CMS muon detector and muon reconstruction with proton-proton collisions at $\sqrt{s} = 13$ TeV", *JINST* **13** (2018) P06015, doi:10.1088/1748-0221/13/06/P06015, arXiv:1804.04528.

[89] CMS Collaboration, "Search for supersymmetry in pp collisions at $\sqrt{s} = 13$ TeV in the single-lepton final state using the sum of masses of large-radius jets", *JHEP* **08** (2016) 122, doi:10.1007/JHEP08(2016)122, arXiv:1605.04608.

[90] CMS Collaboration, "Performance of photon reconstruction and identification with the CMS detector in proton-proton collisions at $\sqrt{s} = 8$ TeV", *JINST* **10** (2015) P08010, doi:10.1088/1748-0221/10/08/P08010, arXiv:1502.02702.

[91] G. Louppe, M. Kagan, and K. Cranmer, "Learning to pivot with adversarial networks", in *Advances in Neural Information Processing Systems*, volume 30, p. 981. 2017. arXiv:1611.01046. doi:10.48550/arXiv.1611.01046.

[92] CMS Collaboration, "The CMS trigger system", *JINST* **12** (2017) P01020, doi:10.1088/1748-0221/12/01/P01020, arXiv:1609.02366.

[93] CMS Collaboration, "Description and performance of track and primary-vertex reconstruction with the CMS tracker", *JINST* **9** (2014) P10009, doi:10.1088/1748-0221/9/10/P10009, arXiv:1405.6569.

[94] CMS Collaboration, "Precision luminosity measurement in proton-proton collisions at $\sqrt{s} = 13$ TeV in 2015 and 2016 at CMS", *Eur. Phys. J. C* **81** (2021) 800, doi:10.1140/epjc/s10052-021-09538-2, arXiv:2104.01927.

[95] CMS Collaboration, "CMS luminosity measurement for the 2017 data-taking period at $\sqrt{s} = 13$ TeV", CMS Physics Analysis Summary CMS-PAS-LUM-17-004, 2018.

[96] CMS Collaboration, "CMS luminosity measurement for the 2018 data-taking period at $\sqrt{s} = 13$ TeV", CMS Physics Analysis Summary CMS-PAS-LUM-18-002, 2019.

[97] J. S. Conway, "Incorporating nuisance parameters in likelihoods for multisource spectra", in *PHYSTAT 2011*, p. 115. 2011. arXiv:1103.0354. doi:10.5170/CERN-2011-006.115.

[98] R. Barlow and C. Beeston, "Fitting using finite Monte Carlo samples", *Comput. Phys. Commun.* **77** (1993) 219, doi:10.1016/0010-4655(93)90005-W.

[99] A. L. Read, "Presentation of search results: the CL_s technique", *J. Phys. G* **28** (2002) 2693, doi:10.1088/0954-3899/28/10/313.

[100] T. Junk, "Confidence level computation for combining searches with small statistics", *Nucl. Instrum. Meth. A* **434** (1999) 435, doi:10.1016/S0168-9002(99)00498-2, arXiv:hep-ex/9902006.

[101] ATLAS Collaboration, CMS Collaboration, and LHC Higgs Combination Group, "Procedure for the LHC Higgs boson search combination in Summer 2011", Technical Report CMS-NOTE-2011-005, ATL-PHYS-PUB-2011-11, 2011.

[102] G. Cowan, K. Cranmer, E. Gross, and O. Vitells, "Asymptotic formulae for likelihood-based tests of new physics", *Eur. Phys. J. C* **71** (2011) 1554, doi:10.1140/epjc/s10052-011-1554-0, arXiv:1007.1727. [Erratum: doi:10.1140/epjc/s10052-013-2501-z].